Supporting Information

Gold Nanoparticle Couples with Entropy-driven Toehold-mediated DNA Strand Displacement Reaction on Magnetic Beads: Toward Ultrasensitive Energy-Transfer-Based Photoelectrochemical Detection of miRNA-141 in Real Blood Sample

Nan Zhang[1a], Xiao-Mei Shi[1a], Hong-Qian Guo[2], Xiao-Zhi Zhao[2], Wei-Wei Zhao[1,3*], Jing-Juan Xu[1] and Hong-Yuan Chen[1*].

1. State Key Laboratory of Analytical Chemistry for Life Science and Collaborative Innovation Center of Chemistry for Life Science, School of Chemistry and Chemical Engineering, Nanjing University, Nanjing 210023, China.

2. Department of Urology, Nanjing Drum Tower Hospital, Medical School of Nanjing University, Institute of Urology, Nanjing University, Nanjing 210008, China.

3. Department of Materials Science and Engineering, Stanford University, Stanford, California 94305, United States.

a. These authors contribute equally.

*E-mail addresses: zww@nju.edu.cn; zww@stanford.edu; hychen@nju.edu.cn

This material includes:

	Au NPs.
Figure S6	Element analysis of the Pdots/ITO electrode via X-ray-photoelectron-spectroscopy before and after assembly of Au NPs.

Table S1. Sequences and stocking solutions of E-TSD reaction.

Name	Modification	Stocking solution	Sequence (5'-3')
Linker	5'-biotin	1×TE buffer B	TTTTTTTTTTTTTTTTTTTTGGATGCA GAGGTTGATTGAATGCCGGGATCCAT CTTTACCAGACAGTGTTA
DNA 1	3'-thiol or 3'-ROX	1×TE buffer A	GGCATTCAATCAACCTCTGCATCCAC ATCCTTTC
DNA 2	None	1×TE buffer B	TCTGGTAAAGATGGATCCCTTATACTA CATACACC
Target	None	1×TE buffer B	UAACACUGUCUGGUAAAGAUGG
Target' (miRNA-141 cognation DNA)	None	1×TE buffer B	TAACACTGTCTGGTAAAGATGG
Fuel	None	1×TE buffer B	TCTGGTAAAGATGGATCCCGGCATTC AATCAACCTCTGCATCC
Separation	3'-biotin	1×TE buffer B	GGGATCCATCTTTACCAGA
Capture	3'-amino	1×TE buffer A	GAGGTTGATTGAATGCC
M	None	1×TE buffer B	UAACACUGUCUCGUAAAGAUGG
D	None	1×TE buffer B	UAACACUGUCUCCUAAAGAUGG
N (miRNA-21)	None	1×TE buffer B	UAGCUUAUCAGACUGAUGUUGA

*1×TE buffer A: diluted 100 times from 100×TE buffer;

1×TE buffer B: 1×TE buffer A containing 100 mM NaCl and 25 mM $MgCl_2$.

2×Binding and Washing (B&W) buffer: 1×TE buffer A containing 2 M NaCl, with or without 0.1% tween 20.

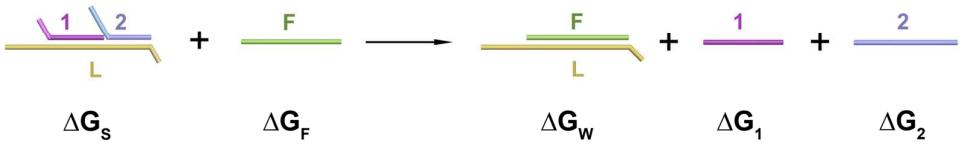

Figure S1. Net reaction equation of the ETSD reaction.

The net equation of the ETSD reaction is illustrated in Figure S1 in order to calculate relating thermodynamic parameters. According to the definition of Gibbs free energy, the Gibbs free energy change of the reaction is expressed as:

$$\Delta G = \Delta H - T\Delta S \quad (1)$$

where ΔH is the change of enthalpy, ΔS is the change of entropy, and T is the thermodynamic temperature. Considering F, DNA 1 and DNA 2 are all single strand nucleic acids, and the base pair in the reactants and the products remain unchanged, thus giving ΔH≈0; on the other hand, the reaction is processed under constant temperature, so the reaction is driven forward by the increment of entropy.

At any moment of the reaction process, the free energy change is:

$$\Delta G = \left(\Delta G_W^\theta + \Delta G_1^\theta + \Delta G_2^\theta\right) - \left(\Delta G_S^\theta + \Delta G_F^\theta\right) + RT \ln Q \quad (2)$$

and Q is the reaction quotient:

$$Q = \left(\frac{[W]}{c^\theta}\right)\left(\frac{[1]}{c^\theta}\right)\left(\frac{[2]}{c^\theta}\right) / \left[\left(\frac{[S]}{c^\theta}\right)\left(\frac{[F]}{c^\theta}\right)\right. \quad (3)$$

where the superscript "θ" means the standard conditions, which in this case representing 1×TE buffer containing 100 mM Na^+ and 25 mM Mg^{2+}, 37 °C, and c^θ=1 M. Meanwhile the standard free energy change is calculated by nucleic acid analysis software NUPACK:

$$\left(\Delta G_W^\theta + \Delta G_1^\theta + \Delta G_2^\theta\right) - \left(\Delta G_S^\theta + \Delta G_F^\theta\right) = -1339.5 \text{ J/mol}$$

When the reaction reaches equilibrium, ΔG= 0, according to equation (2) and equation (3), Q is calculated to be 1.68.

Herein, the initial concentration of S and F are both 10^{-7} M, and assuming the ultimate concentration of W is x M:

$$\frac{x^3}{(10^{-7} - x)^2} = 1.68 \quad (4)$$

X is calculated to be between 9.99×10^{-8} and 9.999×10^{-8}, which means the conversion efficiency of the reaction is more than 99.9%, without regard of the reaction time.

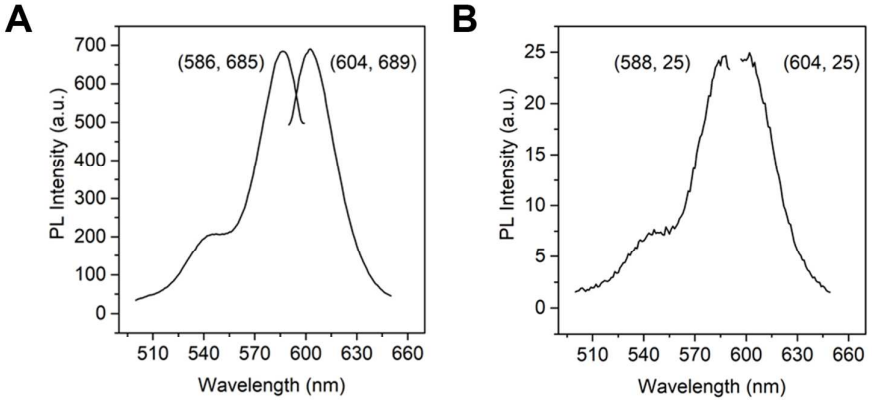

Figure S2. Fluorescent intensity of biotinylated DNA before (A) and after (B) binding with MB.

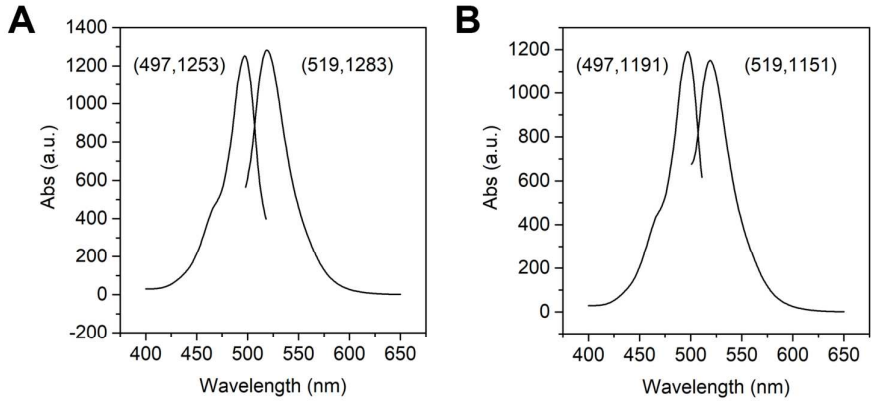

Figure S3. Fluorescent intensity of un-biotinylated DNA before (A) and after (B) binding with MB.

In order to test the binding efficiency and specificity between MB and biotinylated DNA, ROX and FAM was used as fluorescent DNA labels, respectively, and the supernatant before and after binding was measured. The fluorescence emission intensity of biotinylated DNA showed a sharp decrement from 689 to 25, indicating its successful combination with an efficiency of 96.4%, shown in Figure S2. On the other hand, the un-biotinylated DNA labeled with FAM only showed slight change in emission intensity, demonstrated in Figure S3, suggesting the reaction specificity between MB and biotinylated DNA.

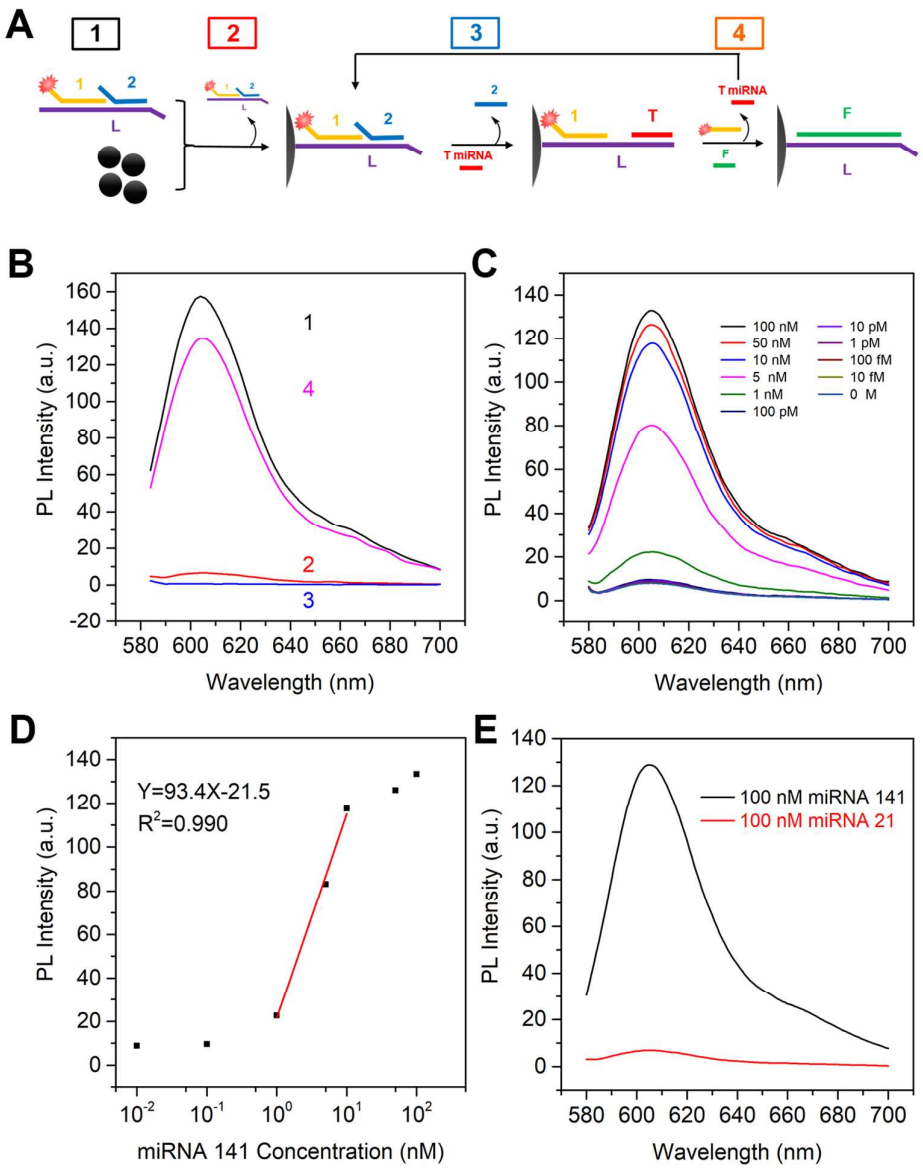

Figure S4. (A) Illustration of the experimental process of ROX-labeled TSD circulation on MB. Step 1: solution of ROX-S; step 2: the supernatant after ROX-S combing with MB and the following magnetic separation; step 3: the supernatant after adding 100 nM target, reacted for 2 h and followed by magnetic separation; step 4: the supernatant after adding 200 nM strand F, reacted for 3 h and followed by magnetic separation. (B) The fluorescent measured at each step. (C) The fluorescent dependency on target miRNA-141 concentration and (D) the corresponding linear range. (E) sequence selectivity investigated by miRNA-21 as an interference.

In order to verify the feasibility of circulation occurrence on MB and investigate the binding and reaction process, ROX-labeled DNA 1 was used in the formation of ternary S, and the supernatant of each step during the procedure was collected and the corresponding fluorescent was measured. As illustrated in Figure S4A, step 1 to step 2 represented the binding process of ternary S on MB,

and the fluorescent decrement indicated the binding efficiency, which calculated from results in Figure S3B, is 95.7%, close to the data of single-stranded DNA. After reaction with 100 nM target miRNA-141 and subsequent magnetic separation, fluorescent of the supernatant was monitored, referred as step 3. In this step, target miRNA-141 liberated DNA 2 through toehold-mediated replacement, however, having no influence on DNA 1, which confirmed by a zero-emission line. Then after washing process and reaction with F, named step 4, the fluorescent recovered to 85.7% of the original value, suggesting the departure of DNA 1 from L and MB, in other words, the successful completion of the TSD reaction on MB. The fluorescent dependency on target concentration was also explored. As shown in Figure S4C and Figure S4D, the fluorescent of step 4 had a positive correlation with the target concentration, and showed a linear range in 10 nM to 1 nM. Additionally, the sequence selectivity was assessed using the interference miRNA-21, with results demonstrated in Figure S4E, validating the anti-interference ability of the detection system.

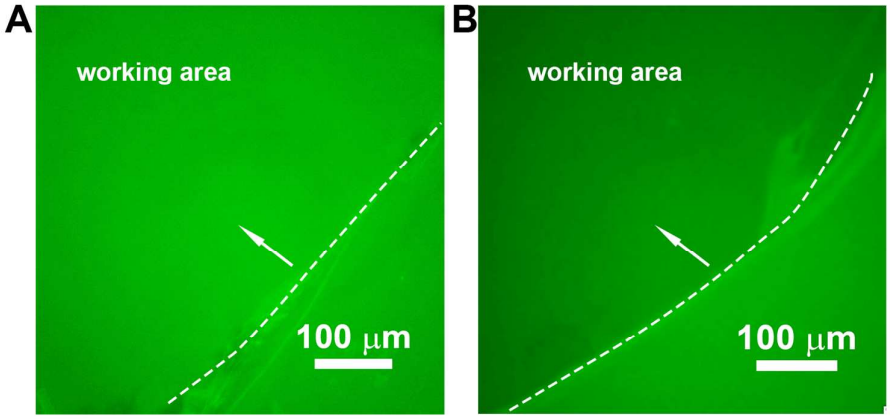

Figure S5. Fluorescent image of the Pdots/ITO electrode before (A) and after (B) immobilization of 100 nM Au NPs-DNA 1, excited by blue light.

Figure S5 depicted the fluorescent image of the fabricated Pdots/ITO electrode before and after anchoring 100 nM Au NPs-DNA 1, under the irradiation of blue light. The left side of the dotted line belonged to the working area, and the right side was covered by colorless scotch tape as a control region. A distinct fluorescent intensity decrement was exhibited in the working area after the immobilization of Au NPs, indicating efficient energy transfer between Pdots and Au NPs, while the tape area remained unchanged.

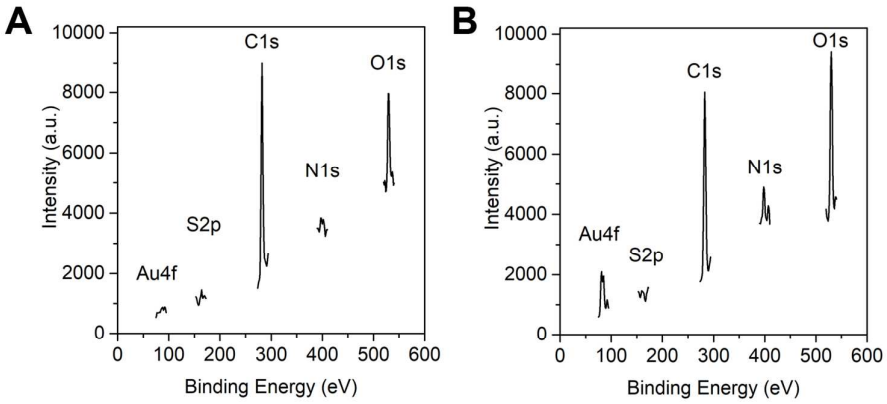

Figure S6. The element analysis via X-ray-photoelectron-spectroscopy before (A) and after (B) assembly of Au NPs.

Table S2. Element proportion change before and after assembly of Au NPs.

	Before (%)	After (%)
C	80.73	68.2 ↓
N	3.26	7.31 ↑
O	14.52	22.94 ↑
S	1.49	0.73 ↓
Au	/	1.00 ↑

Figure S6 showed the results of element analysis results of the Pdots/ ITO electrode before and after assembly of Au NPs recorded by X-ray-photoelectron-spectroscopy (XPS). The bare Pdots/ ITO electrode exhibited a dominant element of C and O, accompanied by small amount of N and S, which come from the monomers of Pdots and PDDA, manifested in Figure S6A. After modification of capture DNA and Au NPs-DNA1, the proportion of N and O increased, brought about by the immobilization N-rich bases and O-rich deoxyribose in oligonucleotides, meanwhile resulting in the decrement of C and S proportion. The most noteworthy change is the increment in the proportion of element Au, which convincingly verify the successful assembly of Au NPs on Pdots/ ITO electrode, shown in Figure S6B and Table S2.

Table S3. Comparison in analytical performance of different miRNA detection methods.

Methods	Target	Linear range	Detection limit	Publication year
Label-free microarray detection[1]	miRNA-96	10- 500 pM	/	2010
Colorimetric PCR-based detection[2]	miRNA-21	0- 50 pM	5 fM	2018
FRET-based fluorescent	miRNA-126	20 fM- 100 pM	3.0 fM	2013

detection[3]				
Silver nanocluster-based fluorescent detection[4]	miRNA-141	1 aM- 1 nM	2 aM	2012
Electrochemiluminescence detection[5]	miRNA-141	1 fM- 100 pM	/	2018
Surface plasmon resonance detection[6]	miRNA-21	10 fM- 100 pM	3 fM	2015
Surface-enhanced raman scattering [7]	miRNA-21 etc.	100 aM –100 pM	100 aM	2014
Label-free electrochemical detection[8]	miRNA-155	5.6 pM-560 nM	1.87 pM	2013
Electrochemical detection[9]	miRNA-122b	10 aM to 1 pM	10 aM	2014
Impedimetric detection[10]	miRNA-26a	30 aM- 10 fM	15 aM	2015
Field-effect transistors-based detection[11]	miRNA-21 etc.	0.1 fM- 1 nM	1 aM	2014
Magnetic relaxation switch sensing-based detection[12]	miRNA-21	5 fM- 0.5 nM	3.36 fM	2016
Photoelectrochemical detection[13]	Let-7a	1 pM- 10 nM	10 fM	2018
Photoelectrochemical detection[14]	miRNA-21	1 fM- 100 pM,	0.2 fM	2016
Photoelectrochemical detection[15]	miRNA-141	0- 10 nM	25.1 aM	2018
Diffusivity-mediated Photoelectrochemical detection[16]	miRNA-155	80 aM- 10 pM	27 aM	2018
Photoelectrochemical detection	miRNA-141	1 fM- 10pM	0.5 fM	this protocol

Table S3 listed the analytical performance of different miRNA detection methods, ranging from traditional microarray detection to dynamically developing optical, magnetic, electrochemical and photoelectrochemical protocols. According to the diversified detection methods and signal amplification strategies, the linear range and detection limit varied from pitomole to zeptomole. In addition, the analytical performance of this protocol was comparable to other photoelectrochemical protocols and other detection methods.

Table S4. Recovery results for the assay of miRNA-141 in whole blood.

Added	Determined	Recovery	RSD (%, n=5)
1 fM	1.05 fM	105%	7.53
10 fM	10.8 fM	108%	6.72
100 fM	103 fM	103%	8.69

1 pM	0.969pM	96.9%	8.17

REFERENCES

(1) Lee, J. M.; Cho, H.; Jung, Y. Fabrication of a structure-specific RNA binder for array detection of label-free microRNA. *Angew. Chem. Int. Ed. Engl.* **2010**, *49*, 8662-8665.

(2) Dong, J.; Chen, G.; Wang, W.; Huang, X.; Peng, H.; Pu, Q.; Du, F.; Cui, X.; Deng, Y.; Tang, Z. Colorimetric PCR-Based microRNA Detection Method Based on Small Organic Dye and Single Enzyme. *Anal. Chem.* **2018**, *90*, 7107-7111.

(3) Tu, Y.; Li, W.; Wu, P.; Zhang, H.; Cai, C. Fluorescence quenching of graphene oxide integrating with the site-specific cleavage of the endonuclease for sensitive and selective microRNA detection. *Anal. Chem.* **2013**, *85*, 2536-2542.

(4) Liu, Y. Q.; Zhang, M.; Yin, B. C.; Ye, B. C. Attomolar ultrasensitive microRNA detection by DNA-scaffolded silver-nanocluster probe based on isothermal amplification. *Anal. Chem.* **2012**, *84*, 5165-5169.

(5) Wang, Y. Z.; Ji, S. Y.; Xu, H. Y.; Zhao, W.; Xu, J. J.; Chen, H. Y. Bidirectional Electrochemiluminescence Color Switch: An Application in Detecting Multimarkers of Prostate Cancer. *Anal. Chem.* **2018**, *90*, 3570-3575.

(6) Qiu, X.; Liu, X.; Zhang, W.; Zhang, H.; Jiang, T.; Fan, D.; Luo, Y. Dynamic Monitoring of MicroRNA-DNA Hybridization Using DNAase-Triggered Signal Amplification. *Anal. Chem.* **2015**, *87*, 6303-6310.

(7) Kang, T.; Kim, H.; Lee, J. M.; Lee, H.; Choi, Y. S.; Kang, G.; Seo, M. K.; Chung, B. H.; Jung, Y.; Kim, B. Ultra-specific zeptomole microRNA detection by plasmonic nanowire interstice sensor with Bi-temperature hybridization. *Small* **2014**, *10*, 4200-4206.

(8) Wu, X.; Chai, Y.; Yuan, R.; Su, H.; Han, J. A novel label-free electrochemical microRNA biosensor using Pd nanoparticles as enhancer and linker. *Analyst* **2013**, *138*, 1060-1066.

(9) Ge, Z.; Lin, M.; Wang, P.; Pei, H.; Yan, J.; Shi, J.; Huang, Q.; He, D.; Fan, C.; Zuo, X. Hybridization chain reaction amplification of microRNA detection with a tetrahedral DNA nanostructure-based electrochemical biosensor. *Anal. Chem.* **2014**, *86*, 2124-2130.

(10) Wan, J.; Liu, X.; Zhang, Y.; Gao, Q.; Qi, H.; Zhang, C. Sensitive impedimetric detection of microRNAs using a hairpin probe based on DNAzyme-functionalized gold nanoparticle tag-initiated deposition of an insulating film on gold electrode. *Sensor. Actuat. B-Chem.* **2015**, *213*, 409-416.

(11) Lu, N.; Gao, A.; Dai, P.; Song, S.; Fan, C.; Wang, Y.; Li, T. CMOS-compatible silicon nanowire field-effect transistors for ultrasensitive and label-free microRNAs sensing. *Small* **2014**, *10*, 2022-2028.

(12) Lu, W.; Chen, Y.; Liu, Z.; Tang, W.; Feng, Q.; Sun, J.; Jiang, X. Quantitative Detection of MicroRNA in One Step via Next Generation Magnetic Relaxation Switch Sensing. *ACS Nano* **2016**, *10*, 6685-6692.

(13) Xiao, M.; Man, T.; Zhu, C.; Pei, H.; Shi, J.; Li, L.; Qu, X.; Shen, X.; Li, J. MoS2 Nanoprobe for MicroRNA Quantification Based on Duplex-Specific Nuclease Signal Amplification. *ACS Appl Mater Interfaces* **2018**, *10*, 7852-7858.

(14) Ma, Z. Y.; Xu, F.; Qin, Y.; Zhao, W. W.; Xu, J. J.; Chen, H. Y. Invoking Direct Exciton-Plasmon Interactions by Catalytic Ag Deposition on Au Nanoparticles: Photoelectrochemical Bioanalysis with High Efficiency. *Anal. Chem.* **2016**, *88*, 4183-4187.

(15) Yu, S.; Wang, Y.; Jiang, L. P.; Bi, S.; Zhu, J. J. Cascade Amplification-Mediated In Situ Hot-Spot Assembly for MicroRNA Detection and Molecular Logic Gate Operations. *Anal. Chem.* **2018**, *90*, 4544-4551.
(16) Hou, T.; Xu, N.; Wang, W.; Ge, L.; Li, F. Truly Immobilization-Free Diffusivity-Mediated Photoelectrochemical Biosensing Strategy for Facile and Highly Sensitive MicroRNA Assay. *Anal. Chem.* **2018**.